Supporting Information

Tailored N-Heterocyclic Perylene Diimide Polymers for Photocatalysis via Molecular Engineering

Yanrong Lu,[a] Zibin Li,[a] Jiajing Feng,*[a] Hong Shang,[a] Bing Sun,[a] and Xueke Liu[b]

[a] School of Science, China University of Geosciences (Beijing), Beijing 100083, P.R. China.
[b] Department of Applied Chemistry, China Agricultural University, Beijing, 100193, P. R. China.
E-mail: fengjiajing@cugb.edu.cn

Table of Contents

1. Materials and Characterization Methods

Materials. All chemicals and solvents were purchased from commercial suppliers and used without further purification unless otherwise specified.

Gel Permeation Chromatography (GPC). Number- and weight-average molecular weights were determined on a PL-GPC 200 instrument at 150°C using trichlorobenzene as eluent.

Fourier Transform Infrared (FT-IR) Spectroscopy. The FT-IR profiles were recorded over the Nicolet iS10. The spectrum was recorded at 4 cm^{-1} resolution with 32 scans, and the resulting data were baseline-corrected.

X-ray Diffraction (XRD). The crystal structure of the photocatalyst was obtained by XRD-6000. The measurements were performed at 40 kV and 1.6 kW using Cu Kα radiation. The data were collected in the 2θ range from 5° to 50°.

X-ray Photoelectron Spectroscopy (XPS). XPS analysis was performed on a ESCALab-250Xi. It is a qualitative and semi-quantitative technique. It was used to analyze the elemental composition and chemical states of elements on the material surface. This information helps deduce hybridization, molecular structure, and chemical bonding. The 1 cm × 1 cm Al foil containing 3 mg of sample was fixed to the sample holder with double-sided conductive tape for measurement. To calibrate for surface adventitious carbon and instrumental shifts, all spectra were referenced by setting the C 1s peak to 284.7 eV.

Surface Area and Porosity Analysis (BET). BET specific surface areas and pore volumes were determined from N_2 adsorption-desorption isotherms collected with a ASAP3020 system at 77 K, pretreatment of sample was activated under vacuum at 120°C for 10 h.

Scanning Electron Microscopy (SEM). SEM imaging of samples were performed on a SU-8010. The powder was ultrasonically dispersed in ethanol, drop-cast onto a Si wafer, dried, and sputter-coated with Au prior to imaging.

Ultraviolet-Visible (UV-Vis) Spectroscopy. UV-Vis adiffuse reflectance spectroscopy (DRS) were measured with Lambda 750. It was used to study the band gap and absorption spectra of the prepared photocatalysts. Diffuse-reflectance spectra (200–800 nm, 1 nm step) were acquired with an integrating sphere using $BaSO_4$ as the reference.

The optical band gap (E_g) of the semiconductor was estimated from the UV–vis DRS absorption edge using the Tauc relation.

$$(\alpha h\nu)^{1/n} = A\,(h\nu - E_g)$$

where $h\nu$ is the photon energy, α the absorption coefficient, and A a proportionality constant. For direct-gap materials n = 1/2, whereas n = 2 is used for indirect-gap semiconductors.

Electrochemical Measurements. Electrochemical properties, including transient photocurrent response, electrochemical impedance spectroscopy (EIS), and Mott-Schottky analysis, were measured using a CHI760E electrochemical workstation.

The working electrode was prepared by dispersing 3 mg of PDI photocatalyst in 1 mL ethanol containing 10 μL Nafion, followed by 20 min ultrasonication; 20 μL of the resultant ink was drop-cast onto 1 × 2 cm ITO glass and dried under an infrared lamp.

A standard three-electrode system was used for the electrochemical tests. A platinum wire served as the counter electrode, and an Ag/AgCl electrode was used as the reference electrode. The electrolyte was a 0.5 mol L^{-1} Na_2SO_4 aqueous solution. A 300 W xenon lamp from Beijing Perfectlight Technology Co., Ltd., equipped with an AM 1.5G filter, was used as the light source. Both the EIS and Mott-Schottky measurements were conducted in the dark.

The flat-band potentials (E_{fb}) relative to the Ag/AgCl electrode were converted to the normal hydrogen electrode (NHE) scale using the formula:

$$E_{fb,\ NHE} = E_{fb,\ Ag/AgCl} + 0.197\ V,$$

For n-type semiconductors, the conduction band minimum (E_{CB}) is generally considered to be positioned 0.1~0.2 eV more negative than the E_{fb} on the NHE scale.

Theoretical calculations. The DFT calculations for the HOMO, LUMO and ESP of PDIs were performed using the Gaussian 16W program. The geometry optimization in the ground state was used the RB3LYP functional with the 6-31G(d, p) basis set. Stuctural models were adopted with two and three PDI structural units, called dimer and trimer, respectively. All geometry optimization was done in the gas phase.

Photocatalytic Degradation Experiment. The photocatalytic degradation activity of the catalysts was evaluated using a multi-channel photocatalytic reactor (CEL-LB70) with Congo red (CR) as the target pollutant. For each test, 10 mg of the catalyst was added to a quartz tube containing 50 mL of a 100 mg L^{-1} CR solution. Before light irradiation, the mixture was stirred in the dark for 30 minutes using the reactor's built-in stirrer to achieve adsorption-desorption equilibrium. Subsequently, photocatalytic degradation was initiated by irradiating the solution with a 500 W xenon lamp at room temperature. Samples (5 mL each) were extracted from the reaction mixture at specific time intervals. Each sample was first filtered through a 0.22 μm aqueous-phase filter membrane and then analyzed by UV-Vis spectrophotometry to determine the remaining concentration of CR.

The photocatalytic degradation data were processed to plot $\ln(C_0/C)$ versus time (t). According to the pseudo-first-order kinetic model, the slope of this plot corresponds to the apparent rate constant (k).

Mechanistic Investigation Experiments. To elucidate the reaction mechanism during photodegradation, scavenger experiments were conducted to identify the primary active species. Methanol (MeOH), tert-butanol (TBA), and p-benzoquinone (BQ) were introduced into the CR solution as scavengers for holes (h^+), hydroxyl radicals ($\cdot OH$), and superoxide radicals ($\cdot O_2^-$), respectively.

2. Synthesis Methods

Synthesis of N-Heterocyclic PDI Polymers (Taking 4,5-PM-PPDI as an example): 0.2202 g (2 mmol) of 4,5-diaminopyrimidine, 0.7816 g (2 mmol) of 3,4,9,10-perylenetetracarboxylic dianhydride, 0.3701 g (2 mmol) of anhydrous zinc acetate and 5.01 g of imidazole were sequentially added to a 250 mL round-bottom flask. The flask was evacuated and refilled with nitrogen three times using a double-manifold Schlenk line and an oil pump, and kept under a static nitrogen atmosphere. The mixture was heated to 180°C with stirring and maintained at this temperature for 12 h. After cooling to ambient temperature, 250 mL of 1 M HCl was added and the suspension was stirred overnight. The precipitate was collected by

vacuum filtration, washed thoroughly with distilled water until the filtrate was neutral, and dried under vacuum at 80 °C for 12 h to yield the crude product.

Purification: the crude solid was suspended in dimethyl sulfoxide, stirred for 10 min and filtered. The solid was washed repeatedly with fresh DMSO until the washings were colourless, then dried again under vacuum at 80 °C for 12 h and ground to a fine powder. The isolated yields of 2,3-P-PPDI, 4,5-PM-PPDI, and 2,3-PZ-PPDI were 76%, 82%, and 89%, respectively.

The resulting polymer was characterized by high-temperature gel-permeation chromatography (GPC) and solid-state ^{13}C nuclear magnetic resonance (^{13}C NMR) spectroscopy to confirm its high molecular weight, structural integrity, and purity.

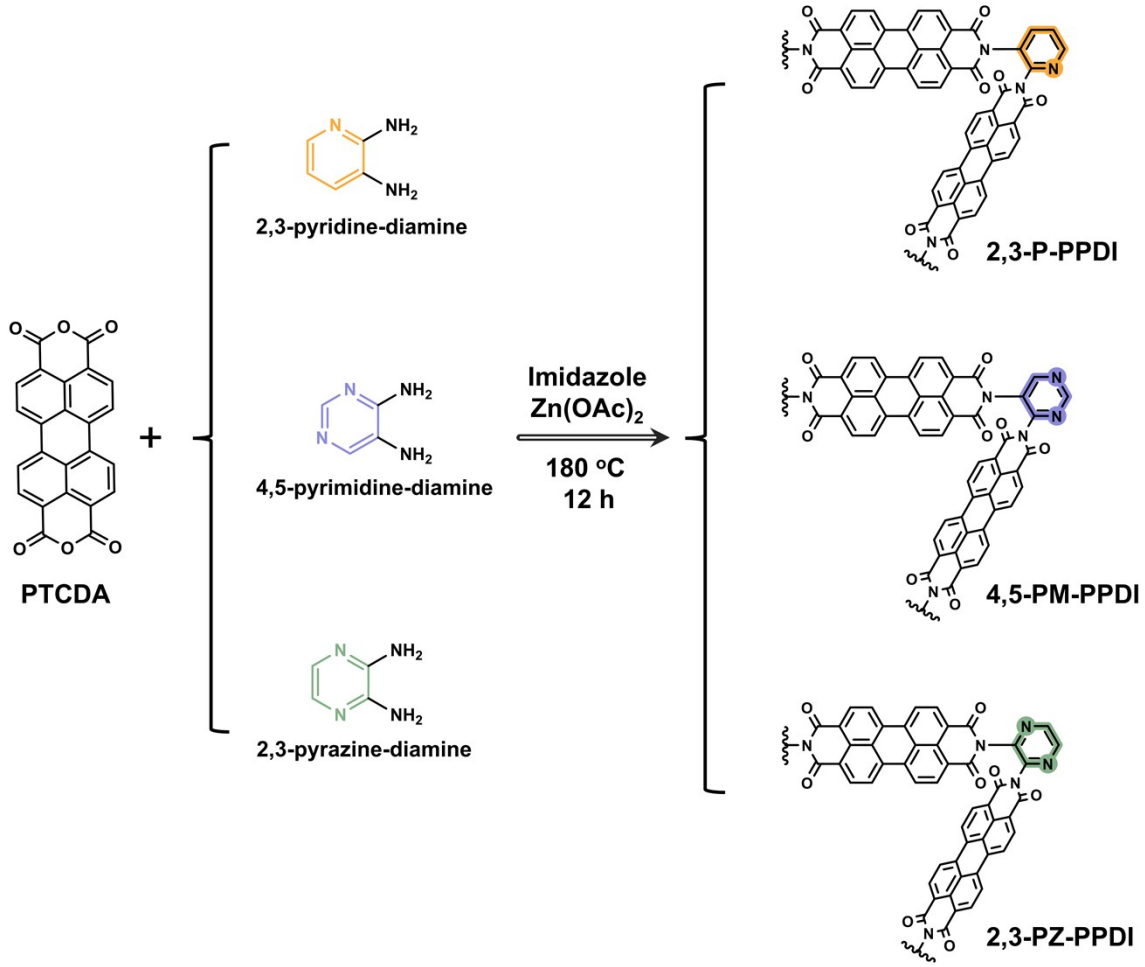

Fig. S1 Schematic illustration of the synthesis of N-heterocyclic PDI polymers.

3. Experimental Results

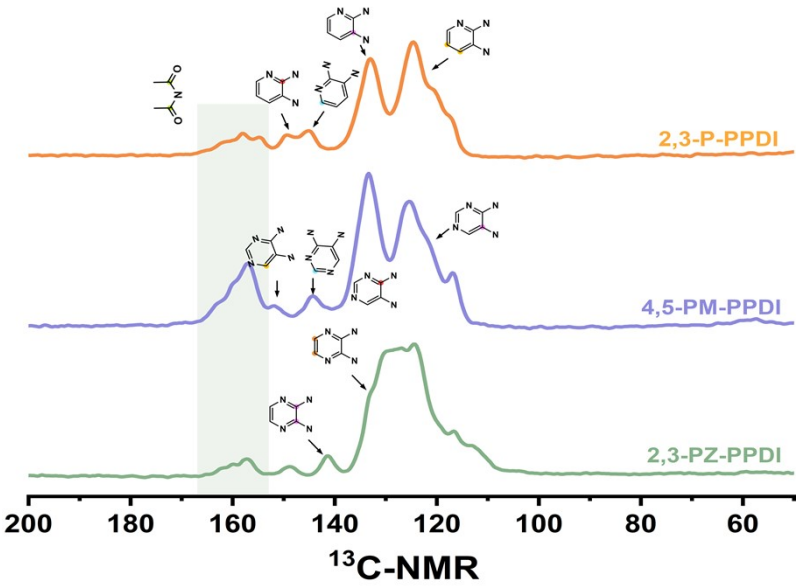

Fig. S2 solid-state ^{13}C NMR spectra of three PDI polymers.

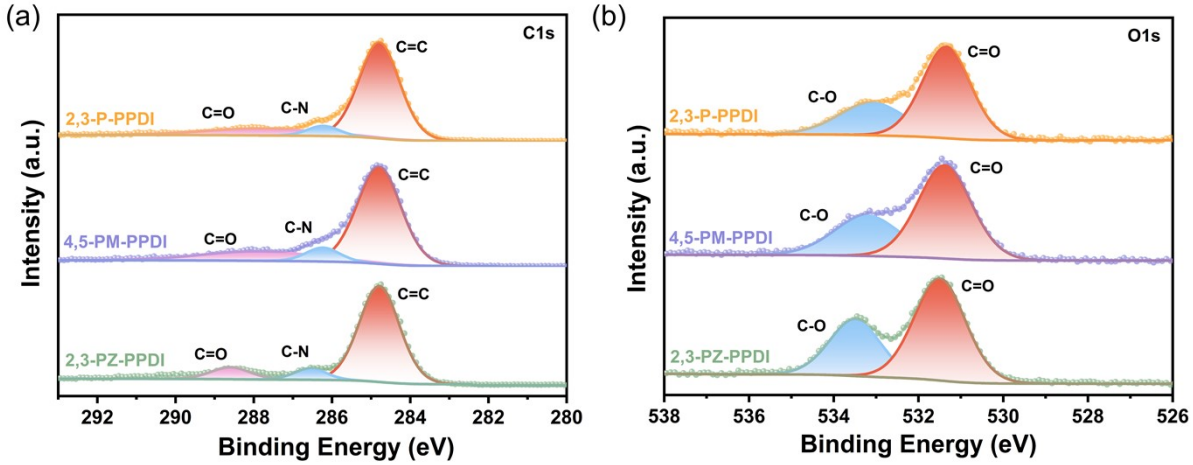

Fig. S3 High-resolution XPS spectra of three PDI polymers.

Table S1 Specific surface area and pore characteristics of three PDI polymers.

	S_{BET} ($m^2\ g^{-1}$)	Pore Volume ($cm^3\ g^{-1}$)	Pore Size (nm)
2,3-P-PPDI	15.8528	0.084057	21.20952
4,5-PM-PPDI	19.4219	0.102968	21.20654
2,3-PZ-PPDI	11.0932	0.055789	20.11642

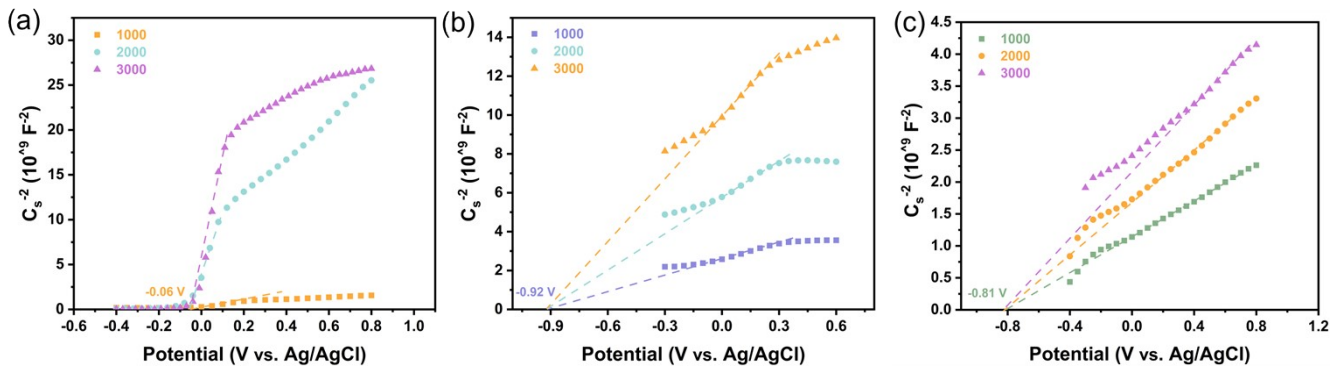

Fig. S4 Mott–Schottky plots of (a) 2,3-P-PPDI, (b) 4,5-PM-PPDI and (c) 2,3-PZ-PPDI measured at different frequencies.

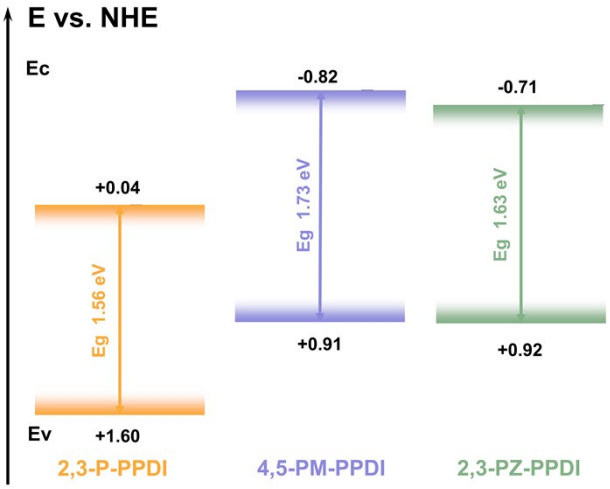

Fig. S5 Energy level diagram of three PDI polymers.

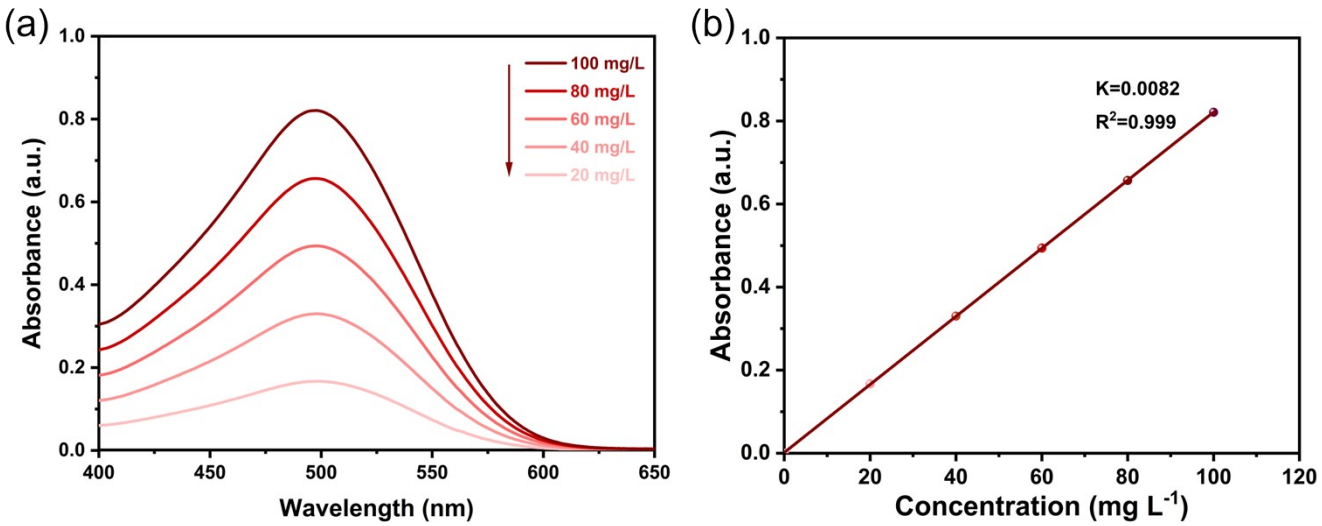

Fig. S6 (a) UV-Vis absorption spectra and (b) absorbance-concentration standard curve of CR at different concentrations.

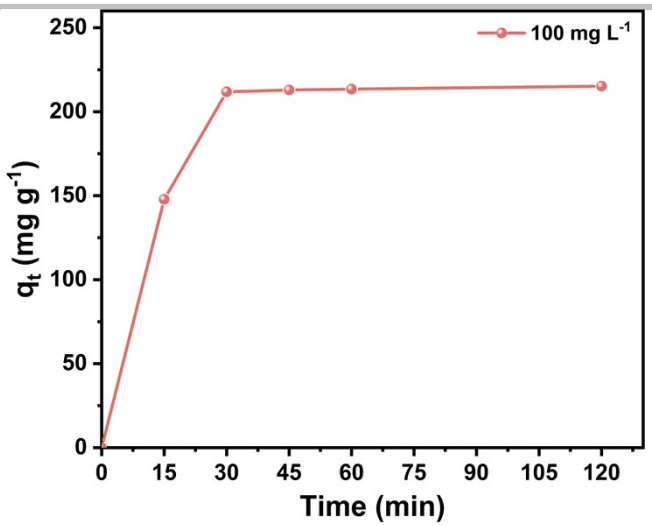

Fig. S7 Adsorption curve of 4,5-PM-PPDI for Congo red.

Table S2 Comparison of the Photocatalytic Properties of PDI Photocatalysts toward Pollutant Degradation

Photocatalysts	Structure and morphology	The amount of catalysts	Targeted pollutant	Concentration of pollutant	Degradation capability	ref.
4,5-PM-PPDI	nanosheets	10 mg	CR	100 mg/L	481 mg/g	This work
PDI-COOH	nanobelts	25 mg	MB RhB	40 mg/L 20 mg/L	About 40 mg/g About 20 mg/g	**1**
sAmi-PDI-HCl	2D layers with flaky	25 mg	MB	1×10^{-5} mol/L	About 4.1 mg/g	**2**
PDI_{SA}/AgBr	rod-shaped structure	30 mg	RhB	10 mg/L	16.3 mg/g	**3**
sL-Ala-PDI	nanobelts	25 mg	MB	5×10^{-5} mol/L	About 37.4 mg/g	**4**

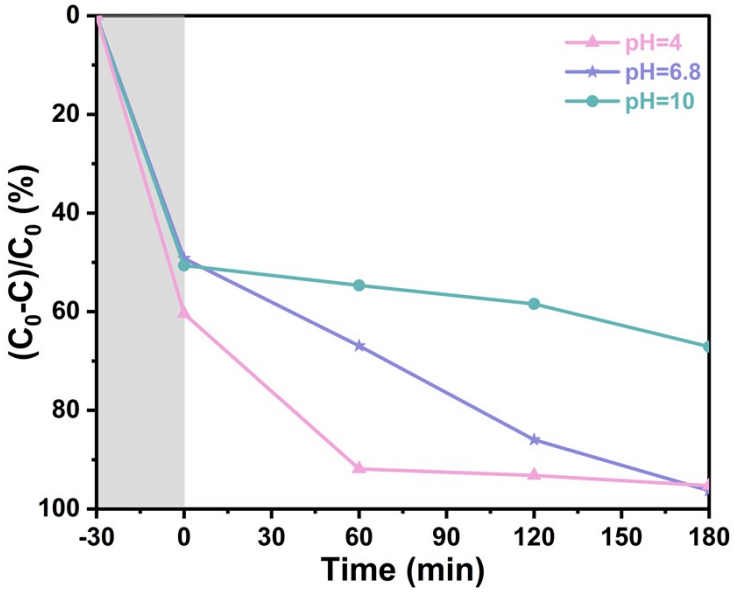

Fig. S8 Degradation of CR of 4,5-PM-PPDI under different pH values.

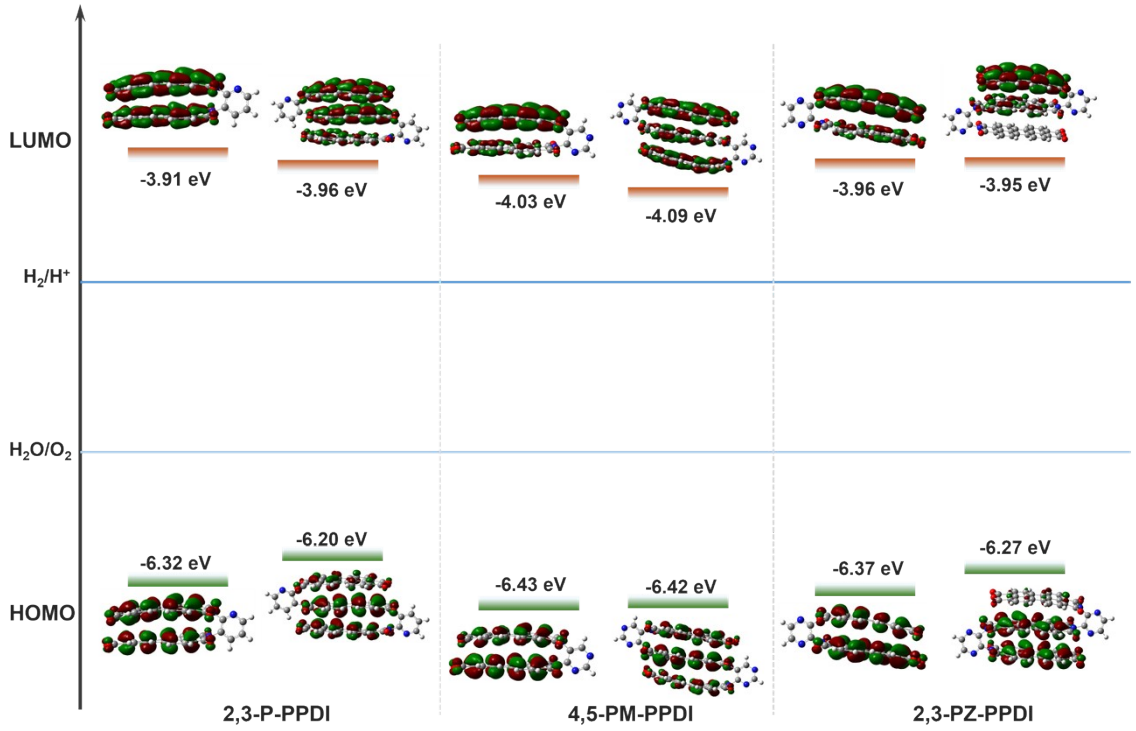

Fig. S9 Optimized geometries, charge distributions, and frontier molecular orbital distributions of the 2,3-P-PPDI, 4,5-PM-PPDI, and 2,3-PZ-PPDI, including both dimers and trimers.

4. References

1. Y. Pu, F. Bao, D. Wang, X. Zhang, Z. Guo, X. Chen, Y. Wei, J. Wang and Q. Zhang, *J. Environ. Chem. Eng.,* 2022, **10**, 107123.
2. H. Li, C. Wang, X. Bai, X. Wang, B. Sun, D. Li, L. Zhao, R. Zong and D. Hao, *Mater. Chem. Front.*, 2020, **4**, 2673-2687.
3. T. Xu, S. Zhang, W. Zhang and L. Shi, *Opt. Mater.*, 2024, **147**, 114656.
4. X. Bai, C. Wang, X. Wang, T. Jia, B. Sun, S. Yang, D. Li, J. Li and H. Li, *Catal. Sci. Technol.*, 2021, **11**, 1899-1913.